Numerical computation of 3D heat transfer in complex parallel convective exchangers using generalized Graetz modes

Charles Pierre, Julien Bouyssier, Frédéric de Gournay, Franck Plouraboué

COMPUTATION OF PARALLEL CONVECTIVE EXCHANGES WITH VERSATILE INLET/OUTLET CONDITIONS USING GENERALIZED GRAETZ MODES

CHARLES PIERRE, JULIEN BOUYSSIER, JÉRÔME FEHRENBACH, FRÉDÉRIC DE GOURNAY, AND FRANCK. PLOURABOUÉ

Abstract. We propose and develop a functional minimization weak-formulation treatment of possibly complex applied input/output conditions which handles either convective, adiabatic, or prescribed temperature at the entrance or the exit of parallel convective exchangers. This formulation permits to re-cast realistic three-dimensional exchangers into a two-dimensional eigenvalue problem which is solved numerically using finite-element. This formulation is robust to mode truncation, offering a huge reduction in computational cost, and providing insight into the most contributing structure to exchanges and transfer. Several examples of exchangers are analyzed to test numerical convergence and illustrate the numerical efficiency of the approach.

1. Introduction

1.1. **Motivation , context, and brief overview.** Parallel convective exchangers are relevant in various applications such as heating or cooling systems [19], haemodialysis [3], and convective exchangers [10]. Since the seminal contributions of Nunge et al. [13, 12] there has been a number of work devoted to parallel convective exchangers in simple two dimensional configurations among which [8], [7] [22] [11], [23][20].

Nevertheless all the abovementioned analysis are limited to two-dimensional configurations (either planar or axi-symmetrical) and convection dominated situations for which the longitudinal diffusion is neglected. The first restriction is mostly associated with the computational cost when dealing with realistic three dimensional (3D) configurations. Nevertheless the increase in computer power will more and more permit the use of direct 3D solutions for predicting exchangers performances [17, 18, 21, 4, 9].

Nevertheless, the focus on convection-dominated situations, albeit justified for traditional convective exchangers, has to be reconsidered in applications such as micro-heat exchangers, where longitudinal diffusion plays a non-negligeable role. This last point, as secondary as it might appear, takes on fundamental implications from the theoretical point of view. First, it has been a recurrent hindrance for the generalisation of Graetz modes as discussed in details in [14]. Secondly, it brings new questions concerning the modeling of convective exchangers, since convective outlet boundary conditions are generally used in this context to describe an approximated purely hyperbolic problem in the longitudinal direction.

Convective boundary conditions, i.e propagating the penultimate temperature value of the considered discrete mesh at the boundary (e.g. in finite difference solutions [17, 18, 21]), permits to circumvent the intrinsic free-boundary nature of exchangers outlet. However the temperature value at the outlet not only depends on the inlet value, but also on the total amount of exchanges arising within the exchanger. Parallel convective exchangers are indeed dealing with a free-boundary coupled problem for which the outlet boundary condition is not known a priori. When longitudinal diffusion is taken into account, the elliptic nature of the operator to be inverted in the longitudinal direction does not permit anymore a convective boundary condition to be chosen. In this case, a new approach has to be found which is the main topic of this paper. We show, in the subsequent sections, how to formulate the exchanger outlet conditions as an unknown field coupled with inlet and outlet tubes solutions. Furthermore, we also show that the only missing outlet unknown are the uniform outlet temperatures at infinity, which can be found from inverting a given linear

Date: February, 2012.

Key words and phrases. Heat and mass transfer, convection diffusion, variational formulation, Graetz mode decomposition, mixed formulation, convective exchangers.

system. At this stage, it is difficult to provide more details on how this new formulation works, it is progressively explained using examples of increasing complexity in section 2.1. The adopted viewpoint is based upon the fact that stationary heat transport equations can be decomposed into generalized Graetz modes in the transverse direction, and functions that solve a simple ordinary differential equation (in this paper exponential functions in the longitudinal direction.

As precedently discussed in [2] it is interesting to extend the use of generalized 2-D Graetz functions for the analysis of realistic exchangers since they permit fast numerical solutions and provide insights on the key features of exchanges modes.

In this contribution we show how complex inlet/outlet configurations can be properly taken into account by a generalized Graetz decomposition solution. The strategy is first to compute numerically the eigenmodes which fulfills both governing equations and lateral boundary conditions, in every considered compartments : inlet, exchanger and outlet.

Given the elements of this base of solutions which are computed in two-dimensions, we settle a functional based upon a L^2 error between the desired boundary conditions and their truncated approximation. The solution is then obtained from minimizing this functional.

Usually the space upon which the solution is formulated is not strictly restrained to the base of admissible solutions which are generally unknown or inextinguishable from the numerical point of view. Here, since the generalized Graetz modes are only computed in two-dimensions (in the third longitudinal dimension their spatial dependence is known analytically), it is possible to first compute the admissible modes from a generalized eigenvalue problem derived from the weak-variational formulation of flux conservation equations. Then, the functional minimization is only associated with the amplitude of each element of the base. This is why the matrix to be inverted in order to find the solution is of very moderate size, since, a moderate number of modes is sufficient to obtain a good approximation.

Section 1.2 provides the necessary self-consistent mathematical background and the specific notations of the considered class of problems.

[2] provide the mathematical framework for dealing with lateral boundary conditions.

Section 2.1 outline the general framework of the method and provide explicit and operational numerical implementation in several realistic class of inlet/outlet configurations using a Graetz spectral decomposition. In section 2.6 the spectral convergence of the method is tested in simple configurations.

Section 3 develops on the numerical implementation of the method using finite-element weak formulation over realistic configurations.

1.2. **State of the art, problem formulation and notation.** We consider the stationary transfer of temperature T inside an exchanger possibly connected along the longitudinal direction, to some arbitrary inlet/outlet conditions. The longitudinal direction is denoted z, whilst the two other transverse coordinates are x and y, and are also re-cast into a transverse vector $\xi = (x, y)$ for which the transverse gradient and divergence operators are denoted $\nabla = (\partial_x, \partial_y)$ and $\mathrm{div} = (\partial_x + \partial_y)$. Convection arises due to a translationally invariant velocity field $\mathbf{v} = v(\xi)\mathbf{e}_z$ independent of z which convects the fluid. For incompressible laminar flow regimes in cylindrical tubes, over a wide range of Reynolds numbers, this velocity field displays a parabolic Poiseuille shape.

In more complex ducts, e.g hexagonal ones [1], the longitudinal velocity $v(\xi)$ is the solution of the following Poisson problem forced by the uniform longitudinal pressure gradient [**?**],

$$\mathrm{div}(\nabla v) = C,$$

where $C = \partial_z p/\mu$. In what follows, we consider laminar fully established longitudinally invariant flow profile, and we suppose that $v(\xi)$ is known. This is compatible with any general assumptions regarding the fluid/gas or arbitrary duct shape. The thermal conductivity k is also assumed to be isotropic and independent of z, but it can vary along the transverse direction $k = k(\xi) \in \mathbb{R}$. The geometry spans over the domain $\Omega \times I$ where Ω is a possibly complex domain in the transverse plane of ξ, and $I \subset \mathbb{R}$ is an interval along the z direction, either finite or semi infinite. The constitutive equation for the convection/diffusion problem reads

$$\mathrm{div}(k\nabla T) + k\partial_z^2 T = v\partial_z T \quad \text{on} \quad \Omega \times I. \tag{1}$$

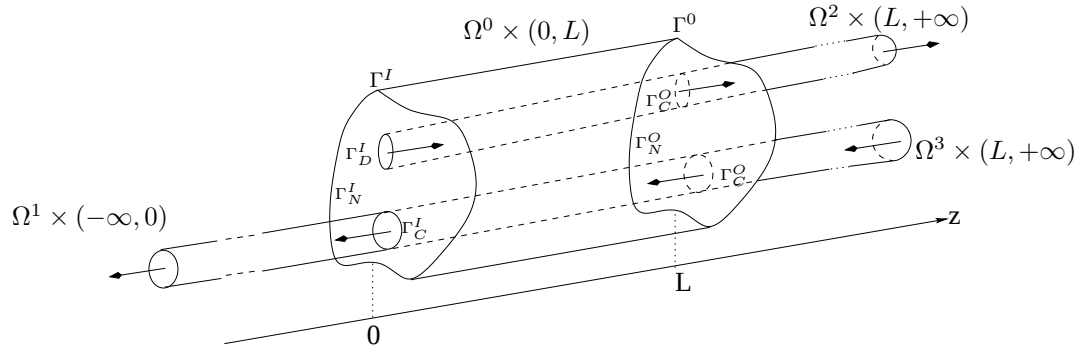

FIGURE 1. Example of configuration. An exchanger in the region $\Omega^0 \times (0, L)$ is coupled with three semi infinite tubes. One inlet tube $\Omega^1 \times (-\infty, 0)$ that has for interface $\Gamma^I_C = \Omega^1 \times \{0\}$. Two outlet tubes $\Omega^{1,2} \times (L, +\infty)$ that have for interface $\Gamma^O_C = \Omega^2 \times \{L\} \cup \Omega^3 \times \{L\}$. In this example we moreover have $\Omega^1 = \Omega^3$. Coupling conditions (4) are imposed at the interface Γ_C. The temperature is prescribed (Dirichlet) on Γ^I_D, modelling a hot fluid injection, whereas a zero flux is imposed on Γ^I_N and Γ^O_N (homogeneous Neumann) modelling an adiabatic condition on the solid sides of the exchanger.

General boundary conditions are imposed and detailed below. Particular solutions to Equation (1) are sought under the form $T = T_\lambda(\xi)\exp(\lambda z)$. This leads to the following definition for the generalized Graetz modes.

Definition 1.1 (Generalized Greatz modess)**.** We consider the following problem, either for a Dirichlet or a Neumann boundary condition: find $\lambda \in \mathbb{R}$ and $T_\lambda \in L^2(\Omega)$ solutions to:

$$\begin{aligned} &\operatorname{div}(k\nabla T_\lambda) + k\lambda^2 T_\lambda = v\lambda T_\lambda \quad \text{on} \quad \Omega, \\ &T_\lambda(\xi) = 0 \quad \text{on} \quad \partial\Omega \qquad \text{or} \qquad k\nabla T_\lambda(\xi)\cdot\mathbf{n} = 0 \quad \text{on} \quad \partial\Omega. \end{aligned}$$

This problem has the form of a generalized eigenproblem. The solutions λ therefore will be called eigenvalues. They form a spectrum Λ whose definition of course depends on the chosen Dirichlet or Neuman boundary condition. The associated eigenfunctions $(T_\lambda)_{\lambda\in\Lambda}$ are the generalized Graetz modes, also depending on the chosen boundary condition.
The mathematical properties of the generalized Graetz modes have been studied in [14, 5, 2]. Generalized Graetz modes have been first used to solve problem (1) on infinite domains in [14]. The use of generalized Graetz modes for finite and semi-infinite domains was then considered in [5]. Extensions to general lateral boundary conditions are presented in [2]. State of the art and notation closely follow those of previous contribution [2] and is not repeated here.(*ca vaudrait le coup en 20 lignes*)
The spectrum Λ decomposes into a double sequence of positive and negative eigenvalues $\Lambda = (\lambda_n)_{n\in\mathbb{Z}^\star}$,

$$-\infty \underset{n\to+\infty}{\longleftarrow} \lambda_n \le \cdots \le \lambda_1 < 0 < \lambda_{-1} \le \cdots \le \lambda_{-n} \underset{n\to+\infty}{\longrightarrow} +\infty.$$

In the Neumann case, $\lambda_0 = 0$ also is an eigenvalue with associated Graetz mode $T_0 = 1$ the constant function, it moreover has multiplicity 2 in case the total flux $\int_\Omega v dx = 0$.
Negative eigenvalues are called downstream and positive ones, upstream, so as the corresponding Graetz modes. In order to clearly distinguish downstream from upstream modes we define in the following

$$\forall\ n \in \mathbb{N}^\star, \quad T^+_n = T_n,\ \lambda^+_n = \lambda_n \quad \text{and} \quad T^-_n = T_{-n},\ \lambda^-_n = \lambda_{-n}.$$

We consider an exchanger in the region $\Omega^0 \times (0, L)$.
The purpose of this contribution is to demonstrate how to use the generalized Graetz modes when applying versatile inlet/outlet conditions to this exchanger. What we mean by versatile conditions is a mixture of Dirichlet, Neumann or Robin conditions applied at the entrance front and/or the output side of the exchanger. But versatile also covers couplings between the entrance and/or the output with semi-infinite tubular inlet/outlets. Such situations are relevant for applications as

illustrated in [19]. A general example of configuration studied here is displayed on Figure 1.
For the sake of simplicity since we concentrate here on inlet/outlet conditions, the analysis and results presented in this paper are restricted to outer lateral Dirichlet boundary conditions, so that for exchangers of longitudinal extent $(0, L)$,

$$T = 0 \quad \text{on} \quad \partial\Omega^0 \times (0, L), \tag{2}$$

along the exchanger. The presented approach is amenable to more complex situations for the applied lateral conditions. General lateral boundary conditions of Dirichlet or Neumann type can be considered following the results in [2]. It would nevertheless provide unnecessary complexity in the presented method at this stage.
The subscripts I and O will be used in the sequel for *Inlet* and *Outlet* respectively. The exchanger has for inlet $\Gamma^I = \Omega^0 \times \{0\}$ and for outlet $\Gamma^O = \Omega^0 \times \{L\}$. The total inlet/outlet domain is $\Gamma = \Gamma^I \cup \Gamma^O$. The input front and output side are partitioned into four different subsets, depending on the type of boundary conditions:

$$\Gamma^{I,O} = \Gamma_D^{I,O} \cup \Gamma_N^{I,O} \cup \Gamma_R^{I,O} \cup \Gamma_C^{I,O}.$$

One will impose respectively Dirichlet, Neumann or Robin boundary conditions on sub-domains D, N and R,

$$\begin{array}{rcll} T(\xi) & = & f(\xi) & \text{on} \quad \Gamma_D, \\ \partial_z T(\xi) & = & g(\xi) & \text{on} \quad \Gamma_N, \\ \partial_z T(\xi) + \alpha(\xi) T(\xi) & = & h(\xi) & \text{on} \quad \Gamma_R. \end{array} \tag{3}$$

The sub-domain Γ_C is reserved for coupling interfaces between the exchanger and semi-infinite tubes. Precisely we consider a collection of semi infinite tubes $\Omega^k \times I^k$ with $\Omega^k \subset \Omega^0$. They are coupled with the exchanger $\Omega^0 \times (0, L)$ either at the inlet, in which case $I^k = (-\infty, 0)$, or at the outlet, in which case $I^k = (L, +\infty)$. An example of such a situation is described on Figure 1. with 3 tubes.

On the interface Γ_C the continuity of fluxes and temperature is imposed,

$$\begin{array}{rcll} T_{\text{left}} & = & T_{\text{right}} & \text{on} \quad \Gamma_C, \\ \partial_z T_{\text{left}} & = & \partial_z T_{\text{right}} & \text{on} \quad \Gamma_C. \end{array} \tag{4}$$

More precisely, we will get at the inlet Γ_C^I, at $z = 0$,

$$T_{\text{left}} = T(\xi, 0^-) \ , \quad T_{\text{right}} = T(\xi, 0^+),$$

whereas at the outlet Γ_C^O, at $z = L$,

$$T_{\text{left}} = T(\xi, L^-) \ , \quad T_{\text{right}} = T(\xi, L^+).$$

Still for the sake of simplicity, we will assume a homogeneous Neumann lateral boundary condition on each semi infinite tube,

$$k \nabla T \cdot \mathbf{n} = 0 \quad \text{on} \quad \partial\Omega^k \times I^k, \tag{5}$$

for $k \geq 1$. A Dirichlet boundary condition could also be considered, as well as a mixture of Dirichlet/Neumann conditions depending on the considered semi infinite tube.

An important note relative to condition (5) is the following. Consider an inlet tube $\Omega^k \times (-\infty, 0)$ in which the fluid flows towards the $z > 0$ direction and thus enters the exchanger at the interface. In this case the temperature $T^{-\infty}$ as $z \to -\infty$ is a data of the problem and will be imposed. Consider now the same inlet tube $\Omega^k \times (-\infty, 0)$ where the fluid now is assumed to flow in the $z < 0$ direction and so leaves the exchanger at the interface. In this case the temperature $T^{-\infty}$ is an unknown of the problem that one wishes to recover. The same considerations hold for the temerature $T^{+\infty}$ as $z \to +\infty$ in outlet tubes but reversed.

2. Resolution method

2.1. **Variationnal formulation.** We want to solve problem (1) for the configuration described in Section 1.2, with specified inlet/outlet conditions (3) and continuous coupling with semi-infinite domains (4).

On the contrary to standard analysis, where one tries to minimize an energy functionnal whose derivative yields the partial differential equation (1) on a space that fulfills the boundary conditions, we chose to perform a quadratic error minimization on the boundary conditions (3) and (4) amongst the solutions of (1). Namely, introduce the functional J as

$$J(T) = \int_{\Gamma_D} |T - f|^2 ds \; + \; \int_{\Gamma_N} |\partial_z T - g|^2 ds \; + \; \int_{\Gamma_R} |\partial_z T + \alpha T - h|^2 ds \\ + \int_{\Gamma_C} |T_{\text{left}} - T_{\text{right}}|^2 ds \; + \; \int_{\Gamma_C} |\partial_z T_{\text{left}} - \partial_z T_{\text{right}}|^2 ds. \tag{6}$$

and minimize J over the set of solution of (1), hereafter denoted V. This space V is known using the Graetz modes, as precised in the following. Consider a solution T to (1), (2), (3), (4) and (5), then it clearly satisifes $T \in V$ and $J(T) = 0$. The reciproque is also true and this two problems are equivalent. Moreover when $J(T) = 0$ then T also is a minimizer of J over V. The continuous problem: find a solution T to (1), (2), (3), (4) and (5) is replaced by the following minimization problem: find $T \in V$ so that $J(T) = \min_{S \in V} J(S)$ and $J(T) = 0$.
Our numerical approach consists in approximating the space V by a finite dimensionnal space V_N of dimension N, namely the one obtained by extracting the first generalized Graetz modes in Definition 1.1 and to minimize J on V_N. Once V_N is defined, we minimize J on V_N. Since J is quadratic, upon choosing a basis of the finite dimensionnal space V_N, the problem may be re-cast into the inversion of the following linear problem: (*avant de passer a la dimension finie peut-on ecrire precisement le probleme en continu ?*) (*J'ai modifié ci dessus, suffisant ? Charles.*)

Definition 2.1 (Finite dimensionnal problem)**.** Let $(e_k)_{k=1\dots N}$ be a basis of the space V_N, decompose,

$$J(T) = m(T, T) + b(T) + c,$$

with m bilinear symetric, b linear and c a constant. Let $\mathbf{M} \in \mathbb{R}^{N \times N}$ and $\mathbf{b} \in \mathbb{R}^N$ be such as $\mathbf{M}_{ij} = m(e_i, e_j)$ and $\mathbf{b}_i = b(e_i)$. Find $\mathbf{x} \in \mathbb{R}^N$ solution of,

$$\mathbf{M}\mathbf{x} = \mathbf{b}. \tag{7}$$

The solution $\mathbf{x}$ of (7), yields $T_N = \sum_{k=1}^{p} x_k e_k$ the minimum point of J over V_n. The fonction T_N is then our approximation of the minimum point of J over V. Also note that with the definition (6), the matrix M moreover is symmetric positive.

The linear system (7) which involves the matrix $\mathbf{M}$ is expected to be of very modest size, typically $N < 100$. The reason for that is that the essential information already is stored within the generalized Graetz modes. Hence, formulation (7) is the main result of this contribution since the proposed spectral approach drastically reduces the numerical complexity of the exchangers mode decomposition.

In the following Sections, we consider different geometries sorted in increasing order of complexity. In Section 2.2, we consider a finite domain with various inlet/outlet boundary conditions. In Section 2.3, a downstream duct is coupled to the finite domain, in Section 2.4, an upstream duct is added, and finally, in Section 2.5, an arbitrary number of downstream /upstream ducts is added. For each configuration, we provide the case-specific functional spaces, and the detailed formulation of matrix $\mathbf{M}$ and vector $\mathbf{b}$.

2.2. **Specified inlet/outlet condition for a single exchanger.** We consider in this section the problem (1) (2) on the exchanger $\Omega^0 \times (0, L)$ together with the specified inlet/outlet conditions (3). An example of such a configuration is displayed on Figure 2.

Applying the ideas of Section 2.1 and the problem of Definition 2.1, we consider V^0 the set of solutions of (1) (2). It is given by,

$$V^0 = \left\{ T(\xi, z) = \sum_{\mathbb{N}^\star} x_n^+ T_n^+(\xi) e^{\lambda_n^+ z} \; + \; x_n^- T_n^-(\xi) e^{\lambda_n^-(z-L)} \right\}, \tag{8}$$

involving the generalized Graetz modes $T_n^\pm$ and the eigenvalues $\lambda_n^\pm$ in Definition 1.1 relatively to the domain Ω^0 and to the Dirichlet boundary condition on $\partial\Omega^0$. A precise study of the mathematical

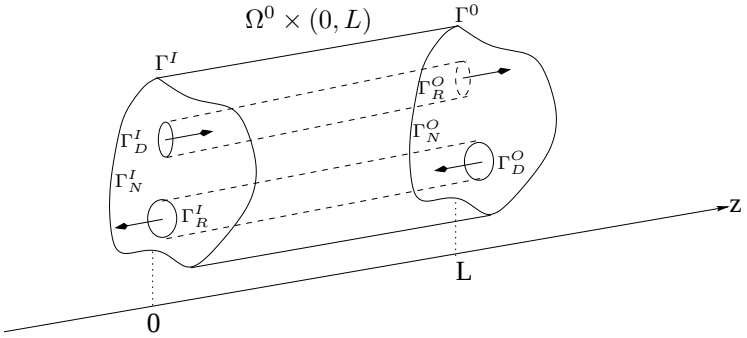

FIGURE 2. Example of exchanger configuration with specified inlet/outlet conditions studied in section 2.2. In this example, we consider Neumann adiabatic insulate conditions at inlet $\Gamma_N^{I,O}$ (solid part), prescribed Dirichlet on $\Gamma_D^{I,O}$ (fluid injection) and Robin boundary conditions on $\Gamma_R^{I,O}$ (fluid outlet).

properties of V^0 is provided in [5]. The finite sub-space V_N^0 that approximates V^0 is obtained by truncating with the N^+ first backward modes and N^- upwards modes:

$$V_N^0 = \left\{ T(\xi,z) = \sum_{n=1}^{N^+} x_n^+ T_n^+(\xi) e^{\lambda_n^+ z} \; + \; \sum_{n=1}^{N^-} x_n^- T_n^-(\xi) e^{\lambda_n^-(z-L)} \right\}.$$

The dimension of V_N^0 is $N = N^+ + N^-$. A straightforward basis of V_N^0 is $(e_k^0)_{1\le k\le N}$ defined as,

$$\begin{cases} e_k^0 : (\xi,z) \mapsto T_k^+(\xi) e^{\lambda_k^+ z} & \text{if } 1 \le k \le N^+ \\ e_{(N^+ + k)}^0 : (\xi,z) \mapsto T_k^-(\xi) e^{\lambda_k^-(z-L)} & \text{if } 1 \le k \le N^- \end{cases} \tag{9}$$

We recast, as stated in Definition 2.1, the minimization of J over V_N^0 into the problem $\mathbf{M}^0 x = \mathbf{b}^0$. In this case the bilinear functionnal m of Definition 2.1 may be decomposed into the sum of two bilinear functionnal $m = m_I + m_O$, the form m^I (resp. m^O) taking in account the effects on the Inlet (resp. Outlet), that is :

$$\begin{aligned} m_I(T,T) = & \int_{\Gamma_D^I} T(\xi,0)^2 + \int_{\Gamma_N^I} \partial_z T(\xi,0)^2 + \int_{\Gamma_R^I} (\partial_z T(\xi,0) + \alpha(\xi) T(\xi,0))^2, \\ m_O(T,T) = & \int_{\Gamma_D^O} T(\xi,L)^2 + \int_{\Gamma_N^O} \partial_z T(\xi,L)^2 + \int_{\Gamma_R^O} (\partial_z T(\xi,L) + \alpha(\xi) T(\xi,L))^2. \end{aligned}$$

In order to compute the matrices $\mathbf{M}^I$ and $\mathbf{M}^O$, let us introduce the eight auxiliary matrices $\mathbf{K}^I_{\pm,\pm}$ and $\mathbf{K}^O_{\pm,\pm}$ whose coefficients are defined if $(a,b) \in \{-,+\}$, $c \in \{I,O\}$, $1 \le i \le N^a$, $1 \le j \le N^b$ by,

$$\mathbf{K}^c_{ab}(i,j) = \int_{\Gamma_D^c} T_i^a T_j^b + \int_{\Gamma_N^c} \lambda_i^a \lambda_j^b T_i^a T_j^b + \int_{\Gamma_R^c} \left(\lambda_i^a + \alpha\right) T_i^a \left(\lambda_j^b + \alpha\right) T_j^b, \tag{10}$$

Note that by definition, the matrices $\mathbf{K}^I_{+-}$ (resp. $\mathbf{K}^O_{+-}$) and $\mathbf{K}^I_{-+}$ (resp. $\mathbf{K}^O_{-+}$) are transposed one of another, so that there are only six different matrices $\mathbf{K}^{I,O}_{\pm\pm}$ to be computed . Then the matrices $\mathbf{M}^I$ and $\mathbf{M}^O$, which are the representation on the base (e_k^0) of the bilinear forms m_I and m_0, are given by:

$$\mathbf{M}^I = \begin{pmatrix} \mathbf{K}^I_{++} & \mathbf{K}^I_{+-}\mathbf{D}_- \\ \mathbf{D}_-\mathbf{K}^I_{+-} & \mathbf{D}_-\mathbf{K}^I_{--}\mathbf{D}_- \end{pmatrix} \quad \mathbf{M}^O = \begin{pmatrix} \mathbf{D}_+\mathbf{K}^O_{++}\mathbf{D}_+ & \mathbf{D}_+\mathbf{K}^O_{+-} \\ \mathbf{K}^O_{+-}\mathbf{D}_+ & \mathbf{K}^O_{--} \end{pmatrix}, \tag{11}$$

where the matrices $\mathbf{D}_\pm$ are the diagonal matrices

$$\mathbf{D}_\pm = \mathrm{Diag}\left(e^{\pm\lambda_1^\pm L}, \ldots, e^{\pm\lambda_N^\pm L}\right) \tag{12}$$

Assembling the matrix $\mathbf{M}^0 = \mathbf{M}^I + \mathbf{M}^O$ thus necessitates:

- the computation of the six matrices $\mathbf{K}^{I,O}_{\pm\pm}$ of size $N^\pm \times N^\pm$,
- the assembly procedure (11).

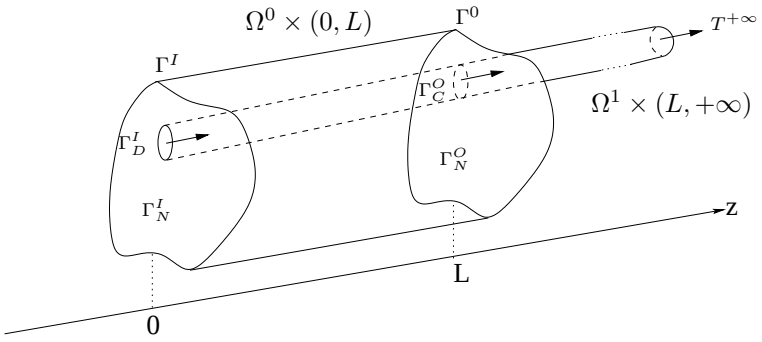

FIGURE 3. Exchanger coupled with an outlet tube of section Ω^1. An upward Dirichlet condition is prescribed on Γ^I_D, an upward and backward Neumann condition is prescribed on $\Gamma^{I,O}_N$ and coupling conditions are prescribed $\Gamma^O_C = \Omega^1 \times \{L\}$ on the interface with the outlet tube. The temp erature $T^{+\infty}$ at infinity is an unknown of the problem.

The left-hand side $\mathbf{b}^0$ similarly decomposes into $\mathbf{b}^0 = \mathbf{b}^I + \mathbf{b}^O$, where the vectors $\mathbf{b}^I$ (resp. $\mathbf{b}^0$) take in account the effects of the Inlet (resp. Outlet) side only and represent the linear forms b^I (resp. b^O) on the basis (e^0_k) of V^0_N, given by:

$$b^I(T) = \int_{\Gamma^I_D} T f ds + \int_{\Gamma^I_N} \partial_z T g ds + \int_{\Gamma^I_R} (\partial_z T + \alpha T) h ds,$$
$$b^O(T) = \int_{\Gamma^O_D} T f ds + \int_{\Gamma^O_N} \partial_z T g ds + \int_{\Gamma^O_R} (\partial_z T + \alpha T) h ds.$$

We introduce the auxiliary vectors $\beta^{I,O}_{\pm} \in \mathbb{R}^{N^\pm}$ defined as,

$$\beta^{I,O}_{\pm}(i) = \int_{\Gamma^{I,O}_D} T^\pm_i \, f \, ds \; + \; \int_{\Gamma^{I,O}_N} \lambda^\pm_i T^\pm_i \, g \, ds \; + \; \int_{\Gamma^{I,O}_R} \left(\lambda^\pm_i + \alpha\right) T^\pm_i \, h \, ds.$$

Finally we obtain,

$$\mathbf{b}^0 = \mathbf{b}^I + \mathbf{b}^O \quad \text{with} \quad \mathbf{b}^I = \left| \begin{array}{c} \beta^I_+ \\ \mathbf{D}_- \beta^I_- \end{array} \right. , \quad \mathbf{b}^O = \left| \begin{array}{c} \mathbf{D}_+ \beta^O_+ \\ \beta^O_- \end{array} \right. ,$$

where $\mathbf{D}_\pm$ are defined in (12).

2.3. **Coupling between an exchanger and an outlet tube.** In this Section, we consider the exchanger $\Omega^0 \times (0, L)$ coupled with an outlet tube $\Omega^1 \times (L, +\infty)$. Their interface is $\Gamma^O_C = \Omega^1 \times \{L\}$. We make the assumption that the flow in this outlet tube occurs in the $z > 0$ direction. An example of such a configuration is described on Figure 3.

We consider two problems. Equations (1) (2) on the exchanger $\Omega^0 \times (0, L)$ on the first hand and equations (1) (5) on the outlet tube $\Omega^1 \times (L, +\infty)$ on the second hand. These two problems are coupled with the coupling conditions (4) on Γ^O_C, and the coupled system is closed considering prescribed boundary conditions (3) on Γ^I and on $\Gamma^O - \Gamma^O_C$.

There are two Graetz problems in this setting. One is set on Ω^0 relatively to the exchanger and then for a homogeneous Dirichlet boundary conditions on $\partial\Omega^0$. The second is set on Ω^1 relatively to the outlet tube and for a homogeneous Neumann boundary conditions on $\partial\Omega^1$. We denote $(T^\pm_n, \lambda^\pm_n)$ the Graetz modes defined for the exchanger and $(t^\pm_n, \mu^\pm_n)$ the Graetz modes defined for the outlet tube. The space of solutions of (1) (2) in $\Omega^0 \times (0, L)$ is exactly V^0, defined in (8) in the previous Section. The space of solutions of (1) (5) in $\Omega^1 \times (L, +\infty)$ is V^1 given by :

$$V^1 = \left\{ T(\xi, z) = x_0 + \sum_{\mathbb{N}^\star} x_n t^+_n(\xi) e^{\mu^+_n (z-L)} \right\}. \tag{13}$$

The downstream Graetz modes t^-_n associated to eigenvalues $\mu^-_n > 0$ do not contribute to the space V^1 since they explode at $z = +\infty$. Moreover, the definition of V^1 involves a constant x_0 which is the uniform temperature value at infinity $x_0 = T^{+\infty}$. This temperature at infinity is an unknwon

of the problem. In order to simplify notations, we shall set $t_0^+ = 1$ the constant fonction and $\mu_0^+ = 0$.
The space of solutions for the total problem naturally is the set of T whose restriction on $z \in (0, L)$ belongs to V^0 and whose restriction on $z \geq L$ belongs to V^1. This set is given by:

$$V = \left\{ T(\xi, z) = \begin{cases} \sum_{\mathbb{N}^\star} x_n^+ T_n^+(\xi) e^{\lambda_n^+ z} \; + \; \sum_{\mathbb{N}^\star} x_n^- T_n^-(\xi) e^{\lambda_n^-(z-L)} & \text{if } 0 \leq z \leq L \\ \sum_{\mathbb{N}} x_n t_n^+(\xi) e^{\mu_n^+(z-L)} & \text{if } L \leq z \end{cases} \right\}.$$

The approximation space V_N is built similarly as in the previous section, we shall keep N^+ (resp. N^-) upward (resp downward) modes of the exchanger and $N^0 + 1$ modes of the outlet tube. The space V_N of dimension $N = N^+ + N^- + N^0 + 1$ admits a basis $(e_k^1)_{1 \leq k \leq N}$ that is built similarly to the one of the space V_N^0 in (9). This basis is built first by extending the basis functions e_k^0 by zero outside the interval $z \in (0, L)$ and then by adding vectors e_k for $N^+ + N^- < k \leq N$ in order to approximate the space V^1. Namely we define $V_N = \text{Span}\left(e_k^1,\ 1 \leq k \leq N\right)$ with,

$$\begin{aligned} &\text{for } 1 \leq k \leq N^+ + N^-, \quad e_k^1(\xi, z) = \begin{cases} e_k^0(\xi, z) & \text{if } 0 \leq z \leq L \\ 0 & \text{if } z > L \end{cases}, \\ &\text{for } 0 \leq k \leq N^O, \quad e^1_{(k+N^- + N^+ + 1)}(\xi, z) = \begin{cases} 0 & \text{if } 0 \leq z \leq L \\ t_k^+(\xi) e^{\mu_k^+(z-L)} & \text{if } z > L \end{cases}. \end{aligned} \tag{14}$$

As previously, we recast the minimization of J over V_N into the problem $\mathbf{M}^1 x = \mathbf{b}^1$. The matrix $\mathbf{M}^1$ to invert is decomposed into,

$$\mathbf{M}^1 = \begin{bmatrix} \mathbf{M}^0 & 0 \\ 0 & 0 \end{bmatrix} + \mathbf{M}_C^O,$$

where $\mathbf{M}^0 = \mathbf{M}^I + \mathbf{M}^O$ is the square matrix of size $N^+ + N^-$ defined in (11) and is associated to the prescribed conditions (3) on Γ. The matrix $\mathbf{M}_C^O$ is related with the couplings at the interface Γ_C^O between the exchanger and the outlet tube whose associated bilinear form is given by

$$m_C^O(T, T) = \int_{\Gamma_C^O} |T_{|\text{left}} - T_{|\text{right}}|^2 + |\partial_z T_{|\text{left}} - \partial_z T_{|\text{right}}|^2 ds.$$

The assembling of $\mathbf{M}_C^O$ necessitates the evaluation of three classes of matrix $\mathbf{Q}_{\pm\pm}$, $\mathbf{R}_{\pm+}$ and $\mathbf{S}+$ whose coefficients are given by, for $(a, b) \in \{-, +\}^2$,

$$\begin{aligned} \mathbf{Q}_{ab}(i,j) &= (1 + \lambda_i^a \lambda_j^b) \int_{\Omega_1} T_i^a T_j^b ds, \quad \text{for} \quad 1 \leq i \leq N^a, \quad 1 \leq j \leq N^b, \\ \mathbf{R}_{a+}(i,j) &= (1 + \lambda_i^a \mu_j^+) \int_{\Omega_1} T_i^a t_j^+ ds, \quad \text{for} \quad 1 \leq i \leq N^a \quad \text{and} \quad 0 \leq i \leq N^O, \\ \mathbf{S}_+(i,j) &= (1 + \mu_i^+ \mu_j^+) \int_{\Omega_1} t_i^+ t_j^+ ds, \quad \text{for} \quad 0 \leq i, j \leq N^O, \end{aligned} \tag{15}$$

Note that $\mathbf{Q}_{+-} = {}^{\mathbf{T}}\mathbf{Q}_{-+}$ and that $\mathbf{Q}_{\pm\pm}$ are matrices of size $N^\pm \times N^\pm$, $\mathbf{R}_\pm$ are matrices of size$N^\pm \times (N^O + 1)$ and finally that the matrix $\mathbf{S}_+$ is of size $(N^O + 1) \times (N^O + 1)$.

The matrix $\mathbf{M}_C^O$ is then defined as,

$$\mathbf{M}_C^O = \begin{bmatrix} \mathbf{M}_+ & \mathbf{C}_+ \\ {}^{\mathbf{T}}\mathbf{C}_+ & \mathbf{S}_+ \end{bmatrix},$$

where $\mathbf{M}_+$ is a square matrix of size $N^+ + N^-$, $\mathbf{C}_+$ is of size $(N^+ + N^-) \times (N^O + 1)$ and $\mathbf{S}_+$ is square of size $(N^O + 1) \times (N^O + 1)$, they are given by the following formulae:

$$\mathbf{M}_+ = \begin{bmatrix} \mathbf{D}_+ \mathbf{Q}_{++} \mathbf{D}_+ & \mathbf{D}_+ \mathbf{Q}_{+-} \\ \mathbf{Q}_{+-} \mathbf{D}_+ & \mathbf{Q}_{--} \end{bmatrix} \quad \text{and} \quad \mathbf{C}_+ = \begin{bmatrix} -\mathbf{R}_{++} \\ -\mathbf{R}_{-+} \end{bmatrix}, \tag{16}$$

where $\mathbf{D}_+$ is the diagonal matrix defined in (12). Hence, matrix $\mathbf{M}^1$ finally reads,

$$\mathbf{M}^1 = \begin{bmatrix} \mathbf{M}^0 & \mathbf{0} \\ \mathbf{0} & \mathbf{0} \end{bmatrix} + \begin{bmatrix} \mathbf{M}_+ & \mathbf{C}_+ \\ {}^{\mathbf{T}}\mathbf{C}_+ & \mathbf{S}_+ \end{bmatrix}. \tag{17}$$

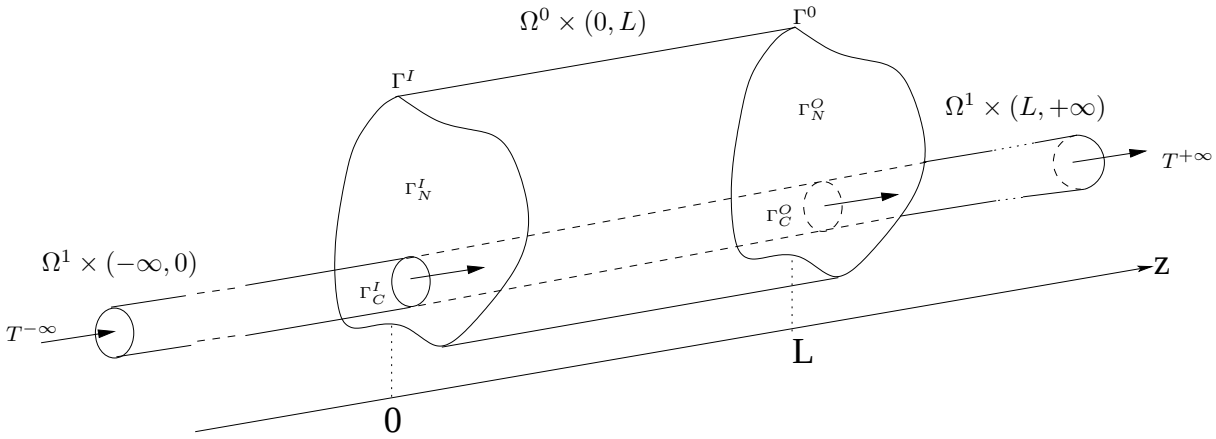

FIGURE 4. Exchanger coupling with one inlet and one outlet tubes and with $\Omega^1 = \Omega^2$ studied in Section 2.4. On this example illustration, an adiabatic frontier $\Gamma_N^{I,O}$ is added. The temperatures at infinity are homogeneous and equals to $T^{\pm\infty}$, $T^{-\infty}$ is a data and $T^{+\infty}$ is an unknown.

The assembling of the left-hand-size is not modified by the coupling of additional constraint, so that it reads $\mathbf{b}^1 = (\mathbf{b}^0, \mathbf{0})$, where $\mathbf{b}^0$ is the vector of size $N^+ + N^-$ defined in (2.2) and is associated with the prescribed Dirichlet and Neumann boundary conditions on Γ.

2.4. **Coupling between an exchanger, an inlet and an outlet tube.** In addition to the previous considered configuration, we now add an inlet tube $\Omega^1 \times (-\infty, 0)$. As in the previous section, we make the assumption that the flow in this inlet/outlet tubes occurs in the $z > 0$ direction.
We now are dealing with three different problems: problem (1) (2) on the exchanger $\Omega^0 \times (0, L)$, problem (1) (5) on the inlet tube $\Omega^1 \times (-\infty, 0)$ and problem (1) (5) on the outlet tube $\Omega^1 \times (L, +\infty)$. These three problems are considered together with,

- coupling conditions (4) at the inlet interface $\Gamma_C^I = \Omega^1 \times \{0\}$ and outlet interface $\Gamma_C^O == \Omega^1 \times \{L\}$,
- prescribed conditions (3) on the remaining part of Γ,
- at $z = -\infty$, the temperature $T^{-\infty}$ is imposed as a constraint of the problem, whereas at $z = +\infty$ the temperature $T^{+\infty}$ is unknown and one free parameter of the problem.

An example of such a configuration is displayed on Figure 4.

The space of solutions for (1) (2) on $\Omega^0 \times (0, L)$ is V^0 defined in (8). The space of solutions for (1) (5) on $\Omega^1 \times (L, +\infty)$ is V^1 defined in (13). Eventually, the set of solutions for (1) (5) on $\Omega^1 \times (-\infty, 0)$ is V^2 given by,

$$V^2 = \left\{ T(\xi, z) = T^{-\infty} + \sum_{\mathbb{N}^\star} x_n t_n^-(\xi) e^{\mu_n^- z} \ , \right\}, \tag{18}$$

where $(t_n^-, \mu_n^-)_n$ are the downstream generalised Graetz modes associated to the domain Ω^1 with Neumann boundary condition. The solution of this coupled problem is search in the set V,

$$V = \left\{ T, \quad T_{|\Omega^0 \times (0,L)} \in V^0, \quad T_{|\Omega^1 \times [L, +\infty[} \in V^1 \quad \text{and} \quad T_{|\Omega^1 \times]-\infty, 0]} \in V^2 \right\}.$$

Keeping our approximation consistent with the one of the previous Sections leads to building a vectorial space V_N of dimension $N = N^+ + N^- + (N^O + 1) + N^I$, whith basis $(e_k^2)_{1 \le k \le N}$ constructed as previously:

$$\text{for } 1 \le k < N - N^1, \quad e_k^2(\xi, z) = \begin{cases} e_k^1(\xi, z) & \text{if } z > 0 \\ 0 & \text{if } z < 0 \end{cases},$$

$$\text{for } 1 \le k \le N^I, \quad e_{k+N-N^I}^2(\xi, z) = \begin{cases} 0 & \text{if } z > 0 \\ t_k^-(\xi) e^{\mu_k^- z)} & \text{if } z < 0 \end{cases}.$$

using the base function e_k^1 defined in (14). The approximation space is then the affine space,

$$V_N = \left\{ T \in T^{+\infty}\chi_{z<0} \oplus \mathrm{Span}\,(e_k,\ 1 \leq k \leq N) \right\}.$$

The matrix $\mathbf{M}$ of linear system (7) decomposes in the following blocks,

$$\mathbf{M} = \begin{bmatrix} \mathbf{M}^1 & \mathbf{0} \\ \mathbf{0} & \mathbf{0} \end{bmatrix} + \mathbf{M}_C^I,$$

where the matrix $\mathbf{M}^1$ on the right-hand-side, defined in (17), is associated with prescribed conditions of functional J and downstream couplings. The second matrix $\mathbf{M}_C^I$ on the right-hand-sides is associated with the inlet coupling, and is precisely associated with the bilinear form m_C^I defined as:

$$m_C^I(T) = \int_{\Gamma_C^I \times \{0\}} |T_{|\mathrm{left}} - T_{|\mathrm{right}}|^2 + |\partial_z T_{|\mathrm{left}} - \partial_z T_{|\mathrm{right}}|^2 ds.$$

Computations show that the matrix $\mathbf{M}_C^I$ has a similar definition than the one of $\mathbf{M}_C^O$, that is it admits the following block-decomposition

$$\mathbf{M}_C^I = \begin{bmatrix} \mathbf{M}_- & \mathbf{0} & \mathbf{C}_- \\ \mathbf{0} & \mathbf{0} & \mathbf{0} \\ {}^T\mathbf{C}_- & \mathbf{0} & \mathbf{S}_- \end{bmatrix},$$

where the square matrix $\mathbf{M}_-$ is of size $N^+ + N^-$, where the matrix $\mathbf{C}_-$ is size $(N^+ + N^-) \times N^I$, and where those matrices are defined as

$$\mathbf{M}_- = \begin{bmatrix} \mathbf{Q}_{++} & \mathbf{Q}_{+-}\mathbf{D}_- \\ \mathbf{D}_-\mathbf{Q}_{+-} & \mathbf{D}_-\mathbf{Q}_{--}\mathbf{D}_- \end{bmatrix} \quad \text{and} \quad \mathbf{C}_- = \begin{bmatrix} -\mathbf{R}_{+-} \\ -\mathbf{R}_{--} \end{bmatrix}, \tag{19}$$

where $\mathbf{D}_-$ is defined in (12), where the matrices $\mathbf{Q}_{\pm\pm}$ are defined in (15), and where the formula for $\mathbf{R}_{\pm-}$ (resp. $\mathbf{S}_-$) are obtained from the formula for $\mathbf{R}_{\pm+}$ (resp. $\mathbf{S}_+$) in (15) upon replacing t^+ by t^-. Finally the matrix $\mathbf{M}$ reads

$$\mathbf{M} = \begin{bmatrix} \mathbf{M}^1 & \mathbf{0} & \mathbf{0} \\ \mathbf{0} & \mathbf{0} & \mathbf{0} \\ \mathbf{0} & \mathbf{0} & \mathbf{0} \end{bmatrix} + \begin{bmatrix} \mathbf{M}_+ & \mathbf{C}_+ & \mathbf{0} \\ {}^T\mathbf{C}_+ & \mathbf{S}_+ & \mathbf{0} \\ \mathbf{0} & \mathbf{0} & \mathbf{0} \end{bmatrix} + \begin{bmatrix} \mathbf{M}_- & \mathbf{0} & \mathbf{C}_- \\ \mathbf{0} & \mathbf{0} & \mathbf{0} \\ {}^T\mathbf{C}_- & \mathbf{0} & \mathbf{S}_- \end{bmatrix},$$

The left-hand-side $\mathbf{b}$ of(7) $\mathbf{b}$ is modified from the previous case due to the presence of the source term $T^{-\infty}$ (imposed temperature at $z = -\infty$),

$$\mathbf{b} = \left| \begin{array}{c} \mathbf{b}^0 \\ 0 \\ \mathbf{b}^{-\infty} \end{array} \right.,$$

where $\mathbf{b}^{-\infty}$ is a N^I dimensional vector whose components are $\mathbf{b}^{-\infty}(i) = T^{-\infty} \int_{\Omega^1} t_i^-(\xi) ds$, and with $\mathbf{b}^0$ defined by (2.2).

2.5. **General case.** In the light of the previous cases it is possible to built the linear system associated with the solution of the general case (7) for an exchanger $\Omega^0 \times (0, L)$ coupled with an arbitrary number of inlet and outlet tubes. One example is illustrated in figure 5.

The exchanger temperature is searched via (8). In each tube, the temperature is searched via,

- (13) for an inlet tube or,
- (18) for an outlet ones.

We precise that in each tube, the first constant term in the decompositions (13), (18) has to be treated:

- either as an unknowon in case the fluid leaves the exchanger and enters the tube at their interface (unknowon temperature at the duct end),
- or conversely as a data in case the fluid enters the exchanger and thus leaves the tube at their interface (prescribed temperature at the duct end).

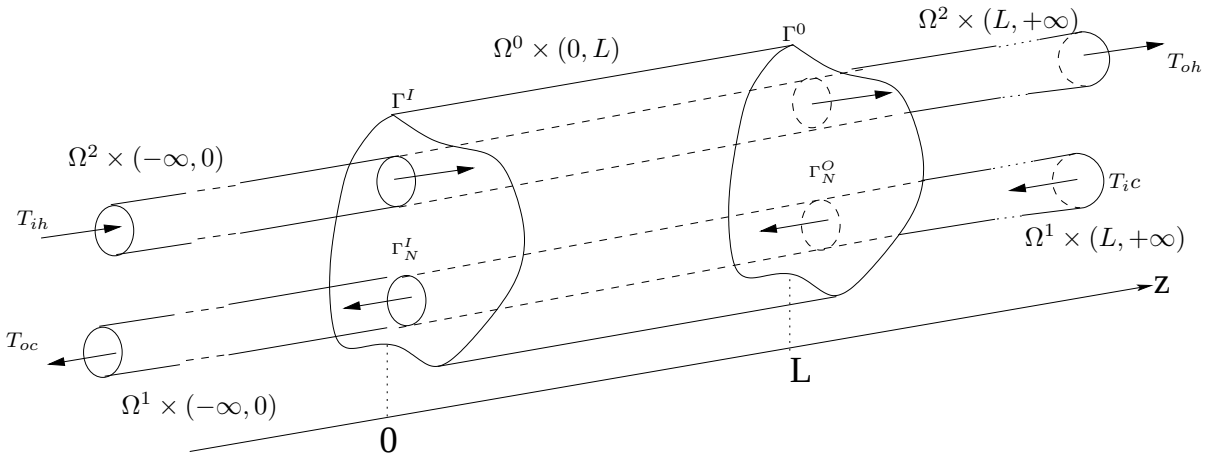

FIGURE 5. Example of a finite domain exchanger coupled with two inlet/outlet tubes. The first tube with section Ω^1 models an injection of hot fluid with input temperature T_{ih} at $z = +\infty$. The second tube with section Ω^2 models an injection of cold fluid with input temperature T_{ic} at $z = -\infty$. The input-hot and input-cold fluid temperatures T_{ih} and T_{ic} are imposed data. After passing through the exchanger $\Omega^0 \times (0, L)$ with prescribed wall temperaure $T_w = 0$, the hot (resp. cold) fluid reaches the output-hot temperature T_{oh} (resp. output-cold T_{oc}) at $z = -\infty$ (resp. $z = +\infty$). The output-hot and output-cold fluid temperatures T_{oh} and T_{oc} are problem unknowns. The two inlet tubes $\Omega^{1,2} \times (-\infty, 0)$ are coupled with the exchanger with conditions (4) on $\Gamma_C^I = (\Omega^1 \cup \Omega^2) \times \{0\}$. Similarly the two outlet tubes $\Omega^{1,2} \times (L, +\infty)$ are coupled with the exchanger with conditions (4) on $\Gamma_C^O = (\Omega^1 \cup \Omega^2) \times \{L\}$. The solid parts Γ_N^I and Γ_N^I of the inlet/outlet are associated with an adiabatic conditions. This configuration is numerically investigated in Sec. 3.3

Considering modes $t_i^{\pm}(\xi)$, $\mu_i^{\pm}$ for each considered inlet/outlet tubes, the matrix M to invert reads,

$$\mathbf{M} = \begin{bmatrix} \mathbf{M}^0 + \mathbf{M}^1 + \cdots + \mathbf{M}^p & \mathbf{C}^1 & \cdots & \mathbf{C}^p \\ {}^T\mathbf{C}^1 & \mathbf{S}^1 & & \\ \vdots & & \ddots & \\ {}^T\mathbf{C}^p & & & \mathbf{S}^p \end{bmatrix}.$$

The block decomposition of M involves,

- the matrix $M^0 = M^I + M^O$ in (11),
- the matrix $\mathbf{M}^i$ are either $\mathbf{M}_+$ in (16) or $\mathbf{M}_-$ in (19) depending on the i^{th} tube to be an inlet or an outlet one,
- similarly the matrix $\mathbf{C}_i$ (resp. matrix $\mathbf{S}_i$) is either $\mathbf{C}_+$ (resp S_+) in (16) or $\mathbf{C}_-$ (resp. $\mathbf{S}_-$) in (19) depending on the i^{th} tube to be an inlet or an outlet one.

2.6. **Spectral convergence.** In this section we discuss the numerical convergence of the functional minimization described in Section 2.1 with the number N of considered generalized Graetz modes. The aim of this section is to analyze the mode truncation independently with some mesh discretization error. For this we consider an axi-symmetric configuration with cylindrical tubes. In this case, a formal analytical computation of modes $T_{\pm i}$ and their related eigenvalue $\lambda_{\pm i}$ is available following the method in [15].

We consider three test cases based on a the same geometry made of two concentric axi-symmetric cylinders. More precisely, for each case, the inlet/outlet tubes section Ω^1 is the unit circle that is embedded in the exchanger section Ω^0 equal to the circle of radius $R = 2$ and with same center 0. he exchanger length is set to $L = 3R = 6$. The flow has the following parabolic Poiseuille profile $v(r) = Pe(1 - r^2)$, where r is the radial coordinate and Pe is the Péclet number which quantify

the ratio between convection/diffusion effects, and is taken equal to $Pe = 10$ is the following. All conductivities in the fluid and the solid are equal to unity. In the following, all the solid inlet/outlet conditions are homogeneous Neumann. Inlet/outlet conditions in the fluid parts are the following.

- **Test case 1:** prescribed temperature $T = 1$ at the inlet on $\Gamma_D^I = \Omega^1 \times \{0\}$ and Robin condition $\partial_z T + \alpha v(\xi) T = 0$ at the outlet $\Gamma_R^O = \Omega^1 \times \{L\}$, as depicted on Figure 2, and with $\alpha = 1/(k_f Pe)$ ($k_f = 1$ denoting the fluig thermal conductivity). This condition expresses a balance between the convective and diffusive heat flux at the outlet, it models a free boundary output condition.
- **Test case 2:** prescribed temperature $T = 1$ at the inlet on Γ_D^I, coupling (4) with an outlet tube on $\Gamma_C^O = \Omega^1 \times \{L\}$, as depicted on Figure 3. In this case the temperature $T^{+\infty}$ at $z = +\infty$ in the outlet tube is an unknown.
- **Test case 3** Coupling with both inlet and outlet tubes using (4) at $\Omega^1 \times \{0\}$ and $\Omega^1 \times \{L\}$, as depicted on Figure 4. In this case the temperature condition $T = 1$ in the inlet $\Omega^1 \times \{0\}$ is replaced by a prescribed temperature $T^{-\infty} = 1$ at $z = -\infty$ in the inlet tube, as previously $T^{+\infty}$ in the outlet tube is an unknown.

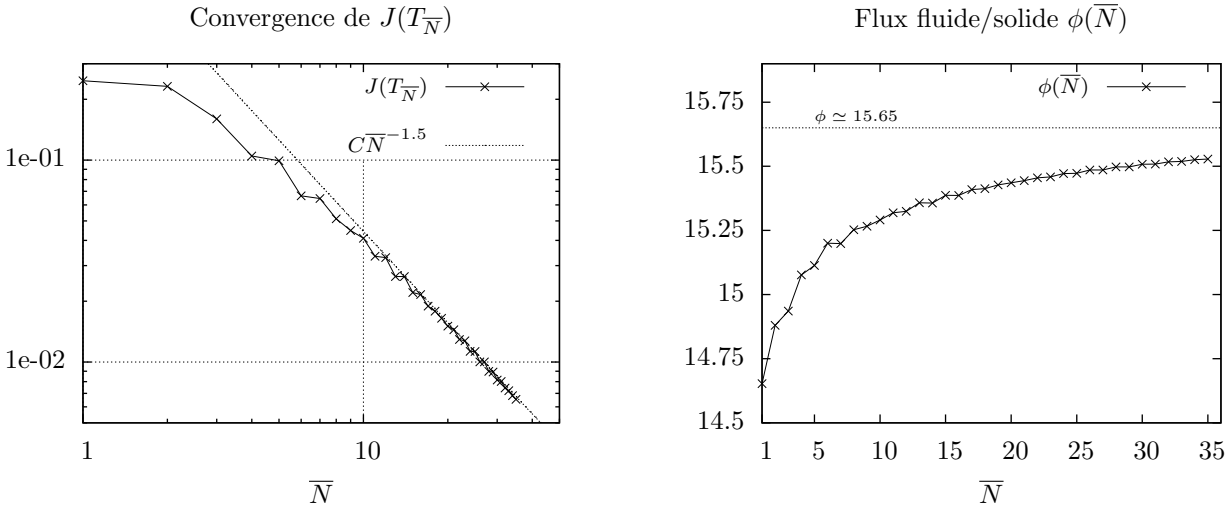

FIGURE 6. Test case 1: convergence of $J(T_N)$ toward zero using bilogarithmic coordinated (left) and the predicted fluid/solid flux convergence $\phi(N)$ (right) versus N_{modes}.

For each test case the linear system $\mathbf{M}x = \mathbf{b}$ in (7) is assembled as presented in Sections 2.2, 2.3 and 2.4 respectively to test cases 1, 2 and 3. It is then solved, providing the minimizer T_N of the functional J over the space V_N. The spaces V_N will always be set so that $N^+ = N^- = N^O = N^I := \overline{N}$. The modal convergence of the method will be investigated with respect to this parameter $\overline{N}$. The total dimension of V_N, respectively to test case 1, 2 and 3, is of $N = 2\overline{N}$, $N = 3\overline{N} + 1$ and $N = 4\overline{N} + 1$.

The minimizer $T_{\overline{N}}$ will be computed for $\overline{N}$ varying between 1 and 35 for test case 1 and between 1 and 28 for test cases 2 and 3. This allows us to analyze the behavior of $J(T_{\overline{N}})$ as $\overline{N} \to +\infty$. Two other quantities of physical interest will be computed using $T_{\overline{N}}$: the fluid/solid heat flux denoted $\phi(\overline{N})$ in the exchanger, (*i.e.* the flux on the interface $\partial\Omega^1 \times (0, L)$) and the temperature as $z = +\infty$ in the outlet tube denoted $T_\infty(\overline{N})$, precisely:

$$\phi(\overline{N}) = \int_0^L \int_{\partial\Omega^1} -k \nabla T_{\overline{N}} \cdot \mathbf{n} dl dz, \quad \text{and} \quad T_\infty(\overline{N}) = \lim_{z \to +\infty} T_{\overline{N}}.$$

The linits ϕ and T_∞ for these two sequences represent the fluid/solid flux in the excnager and the temperature at $z = +\infty$ in the outlet tube for the exact solution T to the considered problem. These limite ϕ and T_∞ have been evaluated, and the relative errors due to truncation are computed

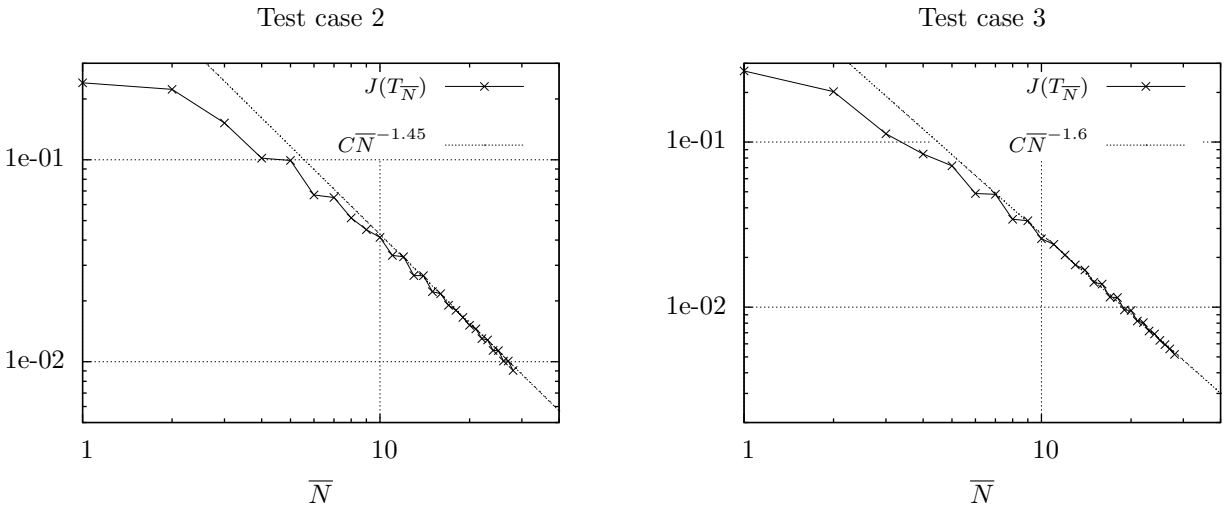

FIGURE 7. Convergence of $J(T_N)$ toward 0 versus N_{modes} in bi-logarithmic scale for test cases 2 and 3.

as,

$$e_\phi(\overline{N}) = \frac{|\phi(\overline{N}) - \phi|}{|\phi|}, \quad e_{T_{+\infty}}(\overline{N}) = \frac{|T_\infty(\overline{N}) - T_\infty|}{|T_\infty|}.$$

Our objective here is to analyze the asymptotic behaviour ot $J(T_{\overline{N}})$, $e_\phi(\overline{N})$ and $e_{T_\infty}(\overline{N})$ as $\overline{N} \to +\infty$.

The convergence of $J(T_{\overline{N}})$ is illustrated on figure 6 (right) for test case 1 and on figure 7 for the test cases 2 and 3. The observed similar linear behavior in bi-logarithmic scale suggest that $J(T_{\overline{N}})$ converges as $O(N^{-3/2})$. Nevertheless, each component of the functional display its own convergence rate and the resulting overall trend is dominate by the worse converging component which is the term associated with the prescribed Dirichlet or the coupling temperature continuity between the inlet/outlet and the exchanger.

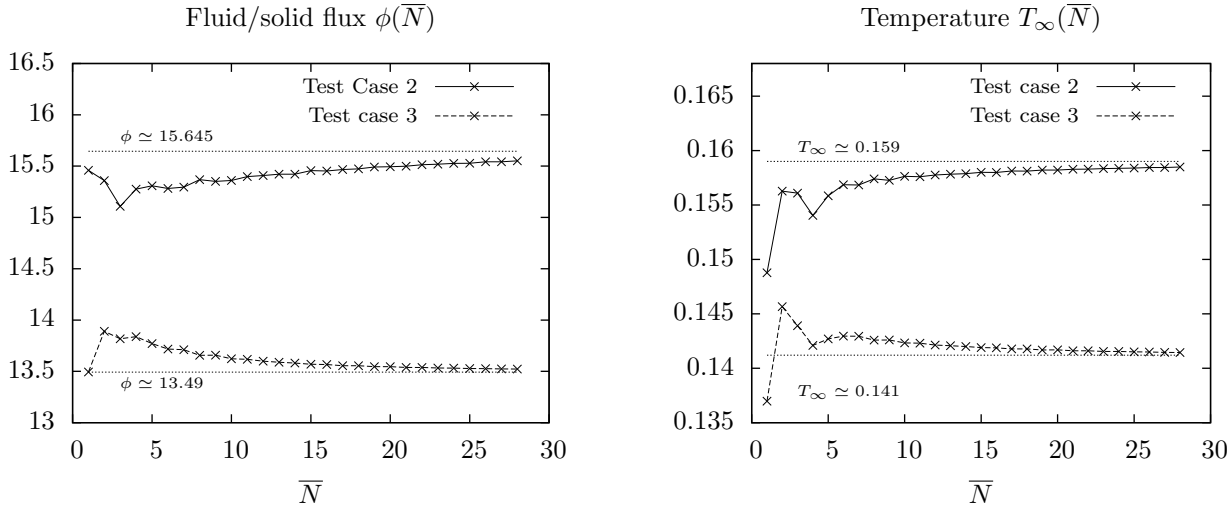

FIGURE 8. Convergence of the predicted fluid/solid flux $\phi(\overline{N})$ (on the left) and of the predicted temperature $T_\infty(\overline{N})$ (on the right) for the test cases 2 and 3.

The convergence of the fluid/solid flux ϕ is illustrated on Fig. 6 (right) for test case 1 and on Fig. 8 (left) for the test cases 2 and 3. All test cases exhibit a rather slow convergence rate with $\overline{N}$: test case 1 has the slowest convergence whereas test case 3 has the fastest. Examinating the relative error $e_\phi(\overline{N})$ shows a geometric convergence $e_\phi(\overline{N}) = O(\overline{N}^{-\alpha})$ with $\alpha \simeq 0.85$, $\alpha \simeq 1$ and

$\alpha \simeq 1.5$ for test case 1, 2 and 3 respectively. Relative errors $e_\phi(\overline{N})$ are given in Tab. 1: even with a very small number of considered Graetz modes $\overline{N}$, the error is within a few percent and is less than 1 percent with 10 modes.

The convergence of the temperature T_∞ at $z = +\infty$ is illustrated on Fig. 8 (right) for the test cases 2 and 3. The asymptotic behavior of the relative error $e_{T_\infty}(\overline{N})$ has also a geometric behaviour, $e_{T_\infty}(\overline{N}) = O(\overline{N}^{-\alpha})$ with $\alpha \simeq 1$ and $\alpha \simeq 1.5$ for test case 2 and 3 respectively. Again, though this convergence rate appears as rather slow, it only holds in the asymptotic region: as displayed on Tab. 1, we obtained an accurate estimation of T_∞ (within a few percent) with very few Graetz modes, and below 1% with 8 modes only.

$e_\phi(\overline{N})$

N	Case 1	Case 2	Case 3
1	0.064	0.012	0 (*sic*)
2	0.049	0.018	0.03
3	0.046	0.034	0.024
5	0.034	0.022	0.02
8	0.025	0.018	0.012
11	0.021	0.016	0.009

$e_{T_\infty}(\overline{N})$

N	Case 2	Case 3
1	0.064	0.030
2	0.017	0.030
3	0.018	0.019
5	0.020	0.010
8	0.010	0.010
11	0.009	0.008

TABLE 1. Relative errors $e_\phi(\overline{N})$ and $e_{T_\infty}(\overline{N})$ associated with the computed fluid/solid flux and computed temperature at $z = +\infty$ respectively on the left and on the right.

3. Numerical illustrations

A first set of numerical examples has been developped in the previous Sec. 2.6 using an analytical (mesh-free) computation of the Graetz modes. This method however is restricted to axi-symmetric geometries. In this section we present numerical results obtained with a finite element formulation, which formulation holds for general geometries. Three cases will be considered. Firstly the test cases 2 and 3 presented in Sec. 2.6 in order to validate the finite element solver. Secondly a non axi-symmetric configuration,

• **Test case 4**: an cylindrical finite exchanger coupled with two upstream and two downsteam tubes.

This last test case serves to demonstrate that the proposed approach can be useful to address realistic complex 3D exchangers geometries, where the 3D temperature field and heat flux are reconstructed.

3.1. Discrete finite element formulation.

The first computational step is the computation of the generalized Graetz modes $T_n^\pm$ and of the associated eigenvalues relatively to each transverse domains Ω^k, $k \geq 0$. We recall the generalized (quadratic) eigen-value problem in Def. 1.1 satisfied by the Graetz modes:

$$\begin{aligned} &\operatorname{div}(k\nabla T_\lambda) + k\lambda^2 T_\lambda = v\lambda T_\lambda \quad \text{on} \quad \Omega, \\ &T_\lambda(\xi) = 0 \quad \text{on} \quad \partial\Omega \qquad \text{or} \qquad k\nabla T_\lambda(\xi)\cdot\mathbf{n} = 0 \quad \text{on} \quad \partial\Omega, \end{aligned}$$

Where Ω either denotes the exchanger section Ω^0 (in which case the boundary condition on $\partial\Omega$ is the homogeneous Dirichlet one) or an input/output semi-infinite tube section Ω^k ($k \geq 1$, in which case the boundary condition on $\partial\Omega$ is the homogeneous Neumann one). We here simply focus on the generic computation of the λ, T_λ. We present the method in the Dirichlet case as presented in [5].

As developped in [14], this quadratic eigenvalue problem can be reformulated into a linear (classical) eigenvalue problem by introducing the supplementary unknown $\mathbf{F}$, which is a vectorial function on Ω. Precisely, we search for $\begin{vmatrix} T \\ \mathbf{F} \end{vmatrix}$ and for $\lambda \in \mathbb{R}$ so that,

$$\begin{vmatrix} k^{-1}vT - k^{-1}\operatorname{div}(\mathbf{F}) \\ k\nabla T \end{vmatrix} = \lambda \begin{vmatrix} T \\ \mathbf{F} \end{vmatrix} .$$

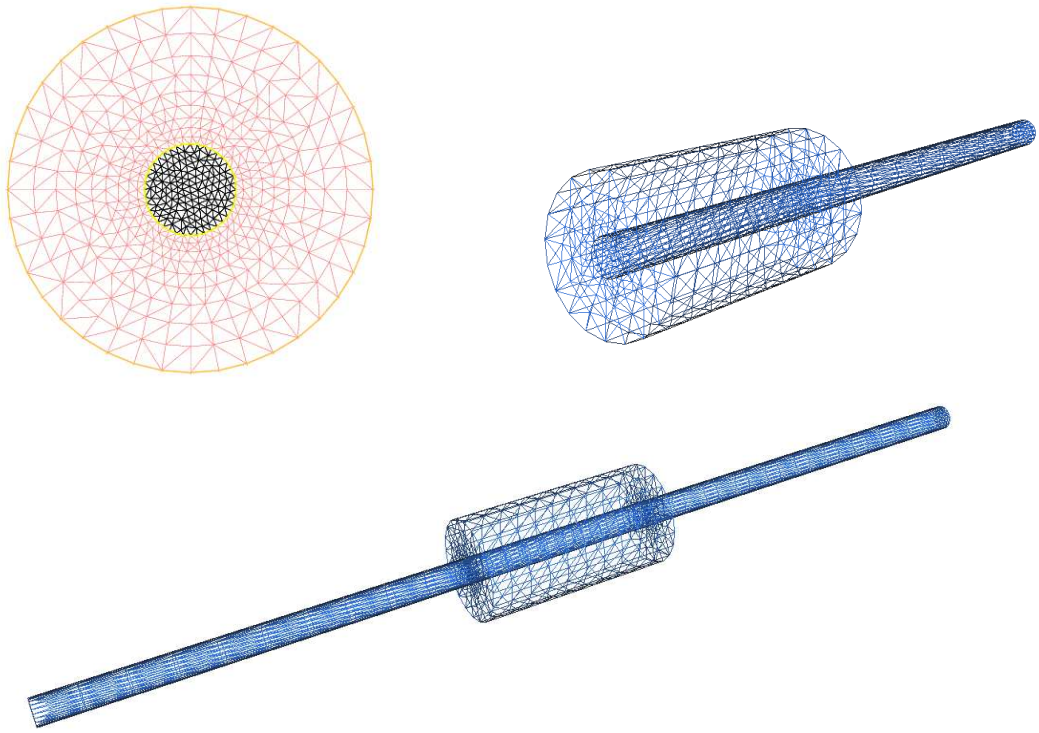

FIGURE 9. Upper left: illustration of the triangle meshes generated by FreeFem++ for test cases 2 and 3. The mesh in black is the triangulation of Ω^1 (fluid part) and the one in red is the triangulation of $\Omega^0 - \Omega^1$ (solid part). The illustrated meshes are intentionally poorly rafined in order to illustrate the conformal connection of the two meshes at the circular frontier $\partial\Omega^I$ (in yellow). Upper right and lower subfigures: 3D meshes obtained from the extrusion of the upper left 2D mesh generated in order to visualise the complete reconstructed solution in the x, y, z directions for test cases 2 (Upper right) and 3 (lower figure).

It has been showed in [5] that the vectorial function $\mathbf{F}$ could be searched under the form $\mathbf{F} = k\nabla U$ for some scalar function $U \in H^1(\Omega)$. As a result we search for $(T, U) \in H_0^1(\Omega) \times H^1(\Omega)$ and for $\lambda \in \mathbb{R}$ so that for all test functions $(t, u) \in H_0^1(\Omega) \times H_0^1(\Omega)$ we have,

$$a_1\big[\ (T,U),(t,u)\ \big] = \lambda\ a_2\big[\ (T,U),(t,u)\ \big],$$

where the bilinear products a_1 and a_2 are defined by,

$$a_1\big[\ (T,U),(t,u)\ \big] = \int_\Omega \big(vTt + k\nabla T\cdot\nabla u + k\nabla t\cdot\nabla U\big)dx,$$
$$a_2\big[\ (T,U),(t,u)\ \big] = \int_\Omega \big(kTt + k\nabla U\cdot\nabla u\big)dx.$$

This problem is approximated using the space $P^k(\mathcal{M})$ of Lagrange-P^k finite element (for $k = 1$ or 2) on a triangulation $\mathcal{M}$ of Ω, as exemplified in figure 9. The discrete formulation simply is, find $(T_h, U_h) \in P_0^k(\mathcal{M}) \times P_0^k(\mathcal{M})$ and $\lambda \in \mathbb{R}$ so that for all test functions $(t, u) \in P_0^k(\mathcal{M}) \times P_0^k(\mathcal{M})$ we have,

$$a_1\big[\ (T_h,U_h),(t,u)\ \big] = \lambda\ a_2\big[\ (T_h,U_h),(t,u)\ \big],$$

and where $P_0^k(\mathcal{M})$ denotes the sub space of $P^k(\mathcal{M})$ composed of all functions vanishing on $\partial\Omega$. The discrete problems takes the form of the following linear system,

$$\mathbf{A}_1 \left| \begin{array}{c} T_h \\ U_h \end{array} \right. = \lambda \mathbf{A}_2 \left| \begin{array}{c} T_h \\ U_h \end{array} \right. , \tag{20}$$

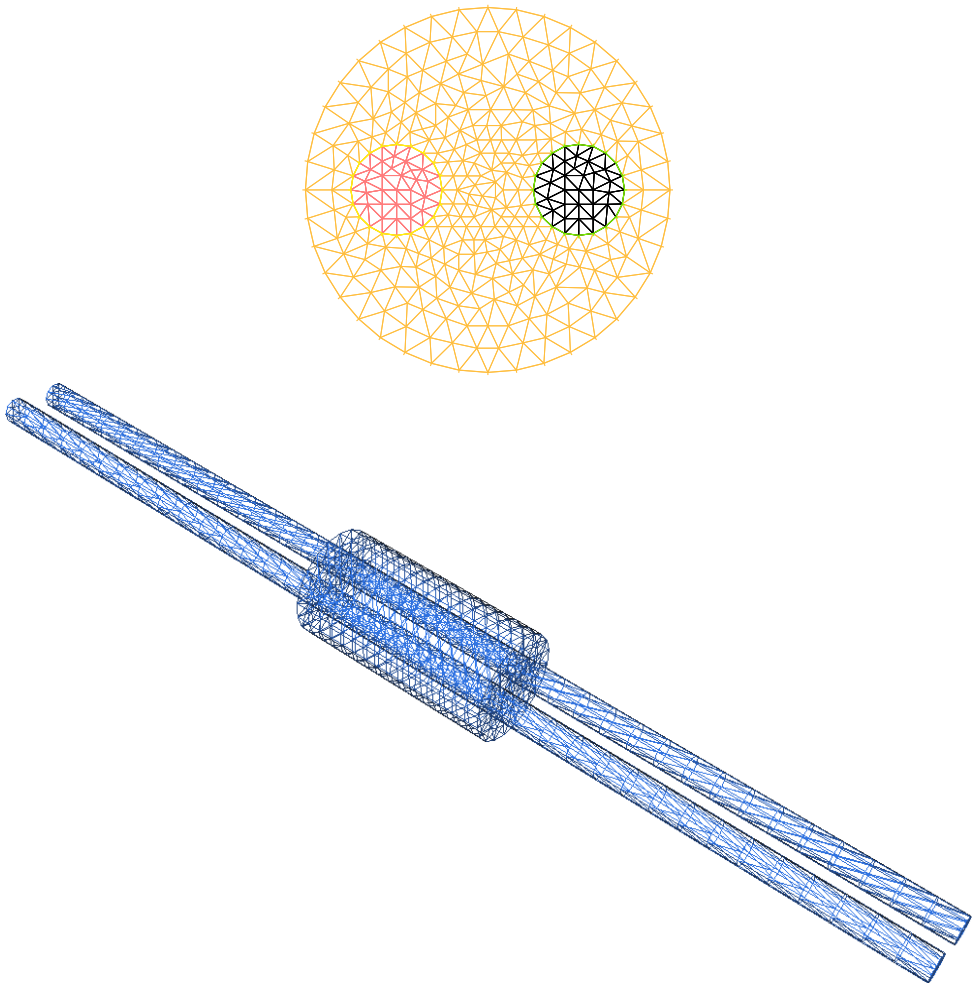

FIGURE 10. Upper sub-figure : Illustration of the finite element mesh generated by FreeFem++ in domain Ω^0 for test case 4. Lower sub-figures: 3D mesh obtained from the extrusion of the upper 2D mesh for 3D reconstruction and visualisation of the solution.

where $\mathbf{A}_1$ and $\mathbf{A}_2$ respectively are the matrices for the bilinear products a_1 and a_2 restricted to $P_0^k(\mathcal{M}) \times P_0^k(\mathcal{M})$ and written considering their classical bases. In practice the assembling of $\mathbf{A}_1$ and $\mathbf{A}_2$ only requires to assemble classical mass and stiffness matrices following the definition of a_1 and a_2. This is done using the finite element library *FreeFem++* [16]. The resolution of the general eigenvalue problem (20) is performed using library *arpack++* [6].
The adaptation of this method to the Neumann case has been further developped in [2]. The technique is the same, only the space of test functions differs. One has to solve (20) with $\mathbf{A}_1$ and $\mathbf{A}_2$ alternatively defined as the matrices for the bilinear products a_1 and a_2 restricted to $P^k(\mathcal{M}) \times P^k(\mathcal{M})$.

The second computational step consists in building the matrix $\mathbf{M}$ and the right hand side $\mathbf{b}$ in (7) associated with the discrete minimization problem in Def. 2.1. Depending on the configuration at ends, this building necessitates various sub-matrices to be evaluated as discussed in section (2.1) i.e $\mathbf{K}$ in (10) and $\mathbf{Q}$, $\mathbf{R}$, and $\mathbf{S}$ in (15). In general, the coefficients of those sub-matrices involve evaluation of integrals of type

$$\int_{\Omega^0} T_i(\xi) T_j(\xi) dx, \quad \int_{\Omega^k} t_i(\xi) t_j(\xi) dx \quad \text{or} \quad \int_{\Omega^k} T_i(\xi) t_j(\xi) dx,$$

where the $T_{i,j}$ denote Graetz modes associated with the excnahger on Ω^0 and where the $t_{i,j}$ denote Graetz modes associated with one given semi-infinite tube on Ω^k. As illustrated on Figs 9 and 10,

the mesh for Ω^k is a conformal sub-mesh of the mesh $\mathcal{M}$ for Ω^0. As a result it is possible (and quite simple) to consider all functions $T_{i,j}$ and $t_{i,j}$ as elements of $P^k(\mathcal{M})$, by extending the $t_{i,j}$ by 0 outside Ω^k. All these integral products then can easily be computed by considering the mass matrix $\mathbf{M}_\Omega$ on $P^k(\mathcal{M})$ and by performing the products,

$$T_i^T \mathbf{M}_\Omega T_j, \quad t_i^T \mathbf{M}_\Omega t_j \quad \text{or} \quad T_{i\Gamma}^T \mathbf{M}_\Omega f t_j. \tag{21}$$

The numerical cost for the assembling of the four matrices $\mathbf{K}$ in (10) and $\mathbf{Q}$, $\mathbf{R}$, and $\mathbf{S}$ in (15) therefore is of one sparce matrix/vector product for each coefficient. This is quite cheap: the assembling of the mass matrix $\mathbf{M}_\Omega$ morover had already been done for the computation of $\mathbf{A}_2$ in (20) and does not need to be repeated here.

The overall computational algorithm thus is the following:

(1) Define the exchanger domain Ω^0 and the inlet/outlet sub-domains Ω^k, then mesh each domain in a conformal way (ie so that the meshes of the Ω^k are sub-meshes of Ω^0's mesh).
(2) Define the inlet/outlet conditions (prescribed boundary conditions (3) and/or inlet/outlet coupling (4) with semi-infinite tubes) and form the space V of solutions as described in Secs 2.2 to 2.5.
(3) Conformly to the definition of the space V, construct the Graetz modes and the associated eigenvalues for each domain Ω^k ($k \geq 0$) using (20).
(4) Built $\mathbf{K}$ from (10), $\mathbf{Q}$, $\mathbf{R}$, and $\mathbf{S}$ from (15) using the mass matrix $\mathbf{M}_\Omega$ as precised in (21).
(5) Built $\mathbf{M}$ and the right hand side $\mathbf{b}$ in (7) and invert $\mathbf{M}\mathbf{x} = \mathbf{b}$.
(6) From the resulting eigenmode decomposition $\mathbf{x}$ reconstruct the complete solution from the chosen solution space V.

3.2. **Finite element solver evaluation.** In this sub-section we consider the axisymmetric test cases 2 and 3 presented in Sec. 2.6 with exactly the same settings. We performed the same simulations as in this section with the finite element solver using both P^1 and P^2 finite elements. The purpose of this section is to validate the finite element method on this axy symmetrical configuration by comparing the results with the analytical ones in Sec. 2.6.

The minimizers $T_{\overline{N}}$ have bben computed for $1 \leq \overline{N} \leq 7$. We hereby present the convergence results of functional minimization $J(T_{\overline{N}})$, infinite temperature $T_\infty(\overline{N})$ and exchange flux at the fluid/solid interface $\phi(\overline{N})$. We observe from figure 11 and figure 12 inspection that the two finite

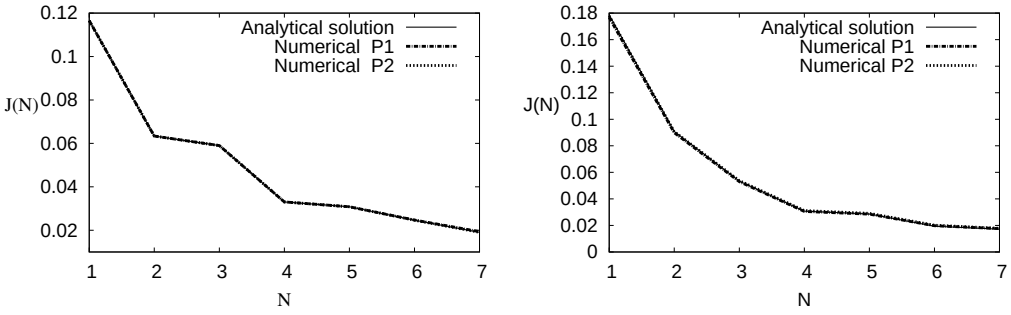

FIGURE 11. Mode convergence for functional $J(N)$ using finite element discretization P^1 & P^2 versus the mode truncation order N for case **2** (left) and case **3** (right) configurations.

element discretizations show very few difference with the analytical predictions. The functional convergence to zero is thus also observed with finite element discretization.

The predicted temperature at infinity $T_\infty(\overline{N})$ observed in figure 12 tends to an asymptotic limit as $\overline{N}$ increases. The comparison between analytical predictions and numerical estimates are close within 1% for P^1 and smaller than 1% for P^2.

The same conclusion holds for the predicted fluid/solid flux $\phi(\overline{N})$. The finite element solver thus is fully validated by this comparison.

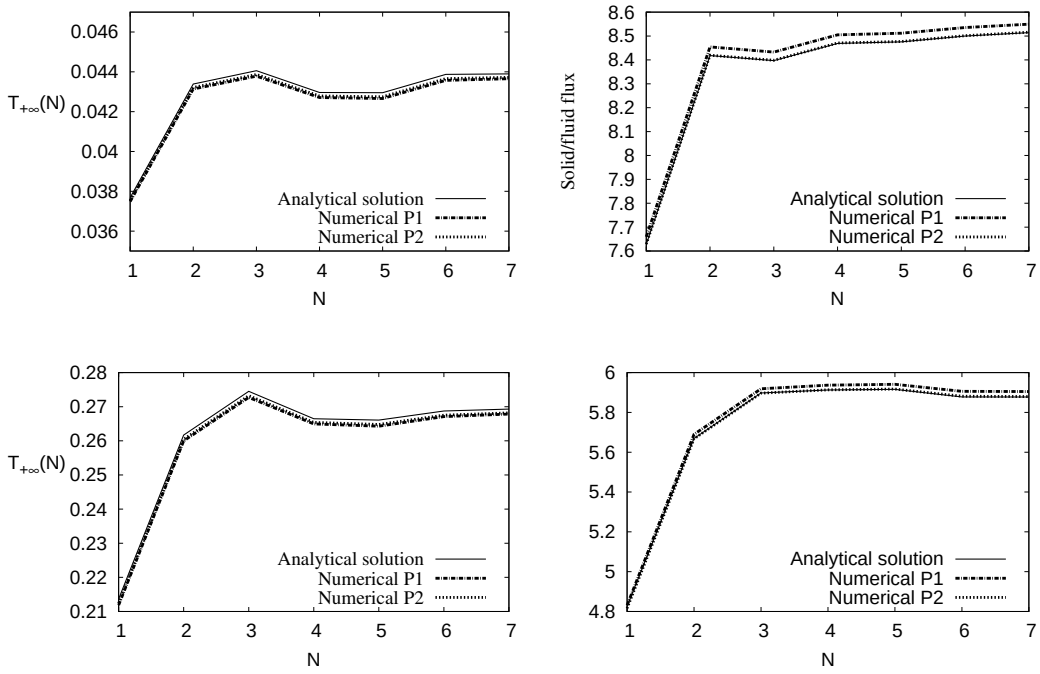

FIGURE 12. Mode convergence for $T_{+\infty}(N)$ (Upper left case : **2**, Lower left case : **3**) and solid/fluid flux exchanges (Upper right case : **2**, Lower right case : **3**) versus mode truncation N.

3.3. **Illustration on a realistic heat exchanger geometry.** In this section we consider the case of a finite exchanger coupled with two inlet/outlet semi-infinite counter-current tubes. This configuration is precisely described on Fig. 5 and the geometry is depicted on Fig. 10.
The two input temperaturess associated with the cold and hot inlets T_{ic}, and T_{ih} are imposed. Two free output temperature have to be found at the far hot and cold tube outlets T_{oc}, and T_{oh}. We denote by T_w the imposed wall temperature on the exchanger boundary $\partial\Omega^0 \times (0, L)$ We here use the dimensionless temperature $T_a = (T - T_w)/(T_{ic} - T_w)$, so that the wall temperature is reset to $T_w = 0$ and the input-hot temperature to $T_{ih} = 1$. Thus, there is only one input parameter, the dimensionless cold inlet temperature $T_{ic} = (T_{ic} - T_w)/(T_{ih} - T_w)$.

Figure **??** shows that, in this case, the functionnal also decreases to zero when increasing the mode truncation, as should be expected. Furthermore we also illustrate a two-dimensional reconstruction of the temrature field in a transverse/longitudinal plane defined by the three axial centre of the two inlet and outlet tubes as well as the exchanger. The temperarure is thus reconstructed in three-dimensional mesh illustrate figure 9 and then represented whithin a plane for illustration. We chose in figure 13 two Péclet number equal to $Pe = 15$ and $Pe = 30$ to illustrate the applicability of the method. The input-cold temperature is set to $T_{ic} = -1$.

4. CONCLUSIONS

We have presented a new approach for the computation of parallel convective exchangers having complex configurations. To our knowledge, the method proposed here consider for the first time, the free boundary nature of exchangers, and how to compute the coupling between inlet and outlet conditions. The use of generalyzed Graetz modes not only permits to map a 3D coomplex problem into a 2D generalyzed eigenvalue problem. It also provides an explicit solution for the base coefficents amplitude from the inversion of a simple linear system defined by the functional minimisation of the coupled inlet/outlet conditions, In finite dimension this functional minimisation always display a unique solution. It might be interesting, in the future to be able to demosntrate the coercivity of the functional definition in functional space, and maybe to use more numerically efficient functionals.

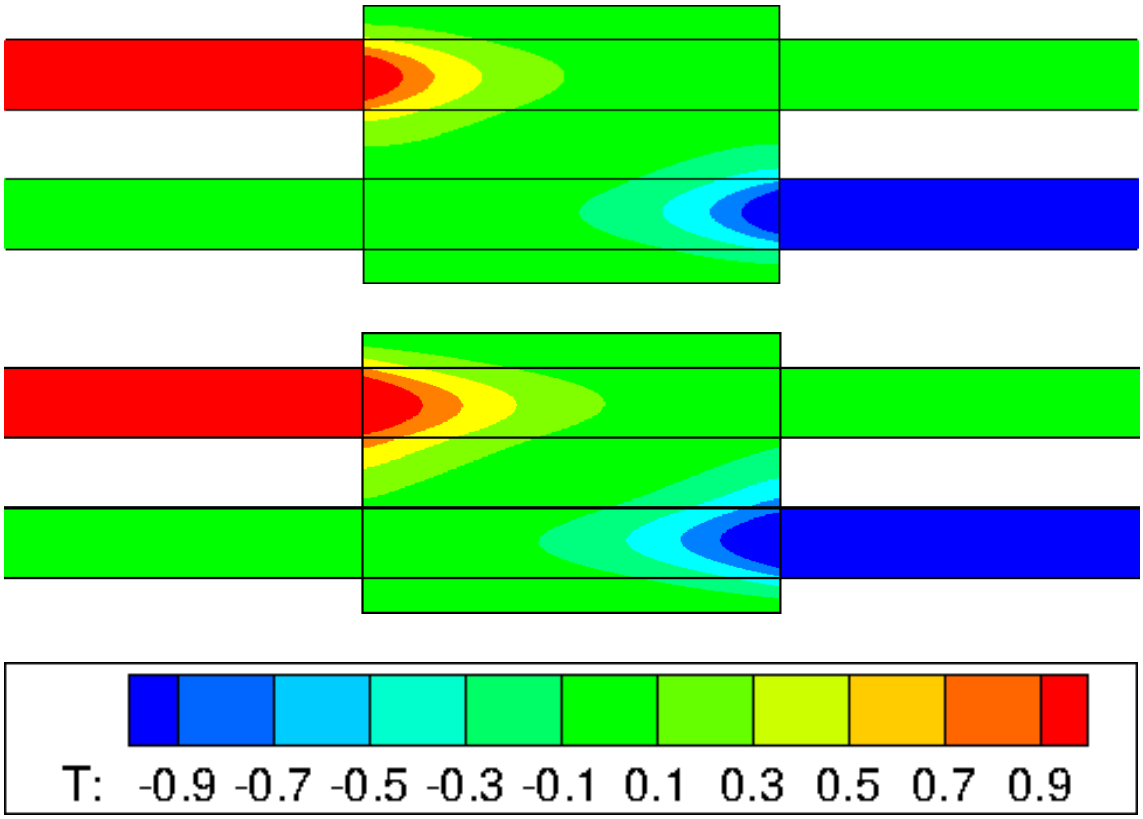

FIGURE 13. Comparison of the temperature field within the exchanger for two value of the Péclet number $Pe = 5$ and $Pe = 50$ for $T_{i,c} = -1$ an exchanger of lenght $L = 4$.

REFERENCES

[1] J. B. Aparecido and Cotta R. M. Laminar flow inside hexagonal ducts. *J. Comp. Mech*, In press(6):93–100, 1990.

[2] J. Bouyssier, C. Pierre, and F. Plouraboué. Mathematical analysis of parallel convective exchangers with general lateral boundary conditions using generalised graetz modes. *Preprint HAL: hal-00667657*, 2013.

[3] Gostoli C. and Gatta A. Mass transfer in a hollow fiber dialyzer. *Journal of Membrane Science*, 6:133–148, 1980.

[4] A.G. Fedorov and R. Viskanta. Three-dimensional conjugate heat transfer in the microchannel heat sink for electronic packaging. *Int. J. Heat Mass Transfer*, 43:399–415, 2000.

[5] J. Fehrenbach, F. De Gournay, C. Pierre, and F. Plouraboué. The Generalized Graetz problem in finite domains. *SIAM Appl. Math.*, 72(1):99–123, 2012.

[6] F.M. Gomes and D. Sorensen. Arpack++. http://www.caam.rice.edu/software/ARPACK/.

[7] C-D. Ho, H-M. Yeh, and W-Y. Yang. Improvement in performance on laminar counterflow concentric circular heat exchangers with external refluxes. *Int. J. Heat and Mass Transfer*, 45(17):3559–3569, 2002.

[8] C.D. Ho, H.M. Yeh, and W.Y. Yang. Double-pass Flow Heat Transfer In A Circular Conduit By Inserting A Concentric Tube For Improved Performance. *Chem. Eng. Comm.*, 192(2):237–255, 2005.

[9] Hong Chungpyo and Asako Yutaka and Suzuki Koichi. Convection heat transfer in concentric micro annular tubes with constant wall temperature . *Int. J. Heat Mass Transfer*, 54(12):5242–5252, 2011.

[10] Kragh J., Rose J., T.R. Nielsen, and Svendsen S. New counter flow heat exchanger designed for ventilation systems in cold climates. *Energy and Buildings*, 39:1151 1158, 2007.

[11] Tu Jr-Wei, Hoa Chii-Dong, and Chuang Ching-Jung. Effect of ultrafiltration on the mass-transfer efficiency improvement in a parallel-plate countercurrent dialysis system . *Desalination*, 242:70 83, 2009.

[12] R. J. Nunge and W. N. Gill. Analysis of heat or mass tranfer in some contercurrent flows. *Int. J. Heat. Mass. Trans.*, 8:873–886, 1965.

[13] R. J. Nunge and W. N. Gill. An analytical study of laminar counter flow double-pipe heat exchangers. *AIChE J.*, 12(2):279–289, 1966.

[14] C. Pierre and F. Plouraboué. Numerical analysis of a new mixed-formulation for eigenvalue convection-diffusion problems. *SIAM Appl. Math.*, 70(3):658–676, 2009.

[15] C. Pierre and F. Plouraboué. Generalised graetz problem: analytical solutions for concentric or parallel configurations. *Preprint HAL:*, 2012.
[16] O. Pironneau, F. Hecht, A. Le Hyaric, and J. Morice. Freefem++. http://www.freefem.org/ff++/.
[17] Qu Weilin and Mudawar, I. Experimental and numerical study of pressure drop and heat transfer in a single-phase micro-channel heat sink. *Int. J. Heat Mass Transfer*, 45(12):2549–2565, 2002.
[18] Qu Weilin and Mudawar, I. Analysis of three-dimensional heat transfer in microchannel heat sinks. *Int. J. Heat Mass Transfer*, 45(19):3973–3985, 2005.
[19] Dušan P. Sekulić R. K. Shah. *Fundamentals of heat exchanger design*. John Wiley and Sons, Ne Jersey, 2003.
[20] M. Vera and A. Li′n. Laminar counter flow parallel-plate heat exchangers: Exact and approximate solutions. *Int. J. Heat. Mass. Trans.*, 53(21-22):4885–4898, 2010.
[21] Weisberg, A. and Bau, H.H. and Zemel, J.N. Analysis of microchannels for integrated cooling. *Int. J. Heat Mass Transfer*, 35:2465–2474, 1992.
[22] H.M Yeh. Numerical Analysis of Mass Transfer in Double-Pass Parallel-Plate Dialyzers with External Recycle. *Chem. Eng. Comm.*, 33:815–821, 2009.
[23] H.M Yeh. Mass Transfer in Cross-Flow Parallel-Plate Dialyzer with Internal Recycle for Improved Performance. *Chem. Eng. Comm.*, 198(11):1366–1379, 2011.

(Charles Pierre)
Laboratoire de Mathématiques et Applications
Université de Pau et du Pays de l'Adour
av. de l'Université BP 1155
64013 PAU Cedex - FRANCE
E-mail address: charles.pierre@univ-pau.fr

(Julien Bouyssier)
Université de Toulouse, INPT, UPS, IMFT (Institut de Mécanique des Fluides de Toulouse), Allés Camille Soula, F-31400 Toulouse, France, and CNRS, IMFT, F-31400 Toulouse, France.
E-mail address: jbouyssi@imft.fr

(J. Fehrenbach)
Institut de Mathématiques de Toulouse, CNRS and Université Paul Sabatier, Toulouse, France
E-mail address: jerome.fehrenbach@math.univ-toulouse.fr

(F. de Gournay)
LMV, Université Versailles-Saint Quentin, CNRS, Versailles, France (gournay@math.uvsq.fr)
E-mail address: frederic@degournay.fr

(Franck. Plouraboué)
Université de Toulouse, INPT, UPS, IMFT (Institut de Mécanique des Fluides de Toulouse), Allés Camille Soula, F-31400 Toulouse, France, and CNRS, IMFT, F-31400 Toulouse, France.
E-mail address: fplourab@imft.fr